Quantitative Proteomics Reveals the Essential Roles of Stromal Interaction Molecule 1 (STIM1) in the Testicular Cord Formation in Mouse Testis*[S]

Bo Zheng‡¶, Dan Zhao‡¶, Pan Zhang‡¶, Cong Shen‡, Yueshuai Guo‡, Tao Zhou‡, Xuejiang Guo‡§, Zuomin Zhou‡§, and Jiahao Sha‡

Testicular cord formation in male gonadogenesis involves assembly of several cell types, the precise molecular mechanism is still not well known. With the high-throughput quantitative proteomics technology, a comparative proteomic profile of mouse embryonic male gonads were analyzed at three time points (11.5, 12.5, and 13.5 days post coitum), corresponding to critical stages of testicular cord formation in gonadal development. 4070 proteins were identified, and 338 were differentially expressed, of which the Sertoli cell specific genes were significant enrichment, with mainly increased expression across testis cord development. Additionally, we found overrepresentation of proteins related to oxidative stress in these Sertoli cell specific genes. Of these differentially expressed oxidative stress-associated Sertoli cell specific protein, stromal interaction molecule 1, was found to have discrepant mRNA and protein regulations, with increased protein expression but decreased mRNA levels during testis cord development. Knockdown of *Stim1* in Sertoli cells caused extensive defects in gonadal development, including testicular cord disruption, loss of interstitium, and failed angiogenesis, together with increased levels of reactive oxygen species. And suppressing the aberrant elevation of reactive oxygen species could partly rescue the defects of testicular cord development. Taken together, our results suggest that reactive oxygen species regulation in Sertoli cells is important for gonadogenesis, and the quantitative proteomic data could be a rich resource to the elucidation of regulation of testicular cord development. ***Molecular & Cellular Proteomics 14: 10.1074/mcp.M115.049569, 2682–2691, 2015.***

From the ‡State Key Laboratory of Reproductive Medicine, Collaborative Innovation Center of Genetics and Development, Department of Histology and Embryology, Nanjing Medical University, Nanjing 210029, China

Received March 3, 2015, and in revised form, July 20, 2015
Published, MCP Papers in Press, July 21, 2015, DOI 10.1074/mcp.M115.049569
Author contributions: X.G., Z.Z., and J.S. designed research; B.Z., D.Z., P.Z., C.S., and Y.G. performed research; B.Z., T.Z., X.G., Z.Z., and J.S. analyzed data; B.Z., X.G., Z.Z., and J.S. wrote the paper, which was read and approved by all the authors.

Male gonadogenesis is a complex process that requires the formation and assembly of several cell types that come together to form a functional organ. These cell lineages coordinate to maintain testicular cord development but do not differentiate independently (1, 2). Shortly after the activation of *Sox9*, when the genital ridges are still long and very thin, pre-Sertoli cells start to aggregate around germ cell clusters and form cords; they are then referred to as Sertoli cells. Partitioning of this mass of cells into cord-forming units coincides with endothelial cell invasion and expansion of interstitial space (3, 4). In mice, organization of the testicular cords begins with aggregate of germ cell and Sertoli progenitors in the gonad. Previous studies using confocal analysis and three-dimensional modeling have reported that testicular cord formation involves three basic steps (5, 6): pre-Sertoli cells and germ cells coalesce between 10.5 and 12.5 days post coitum (dpc)[1]; cords partition at 12.5 dpc with a clear basal lamina surrounding the cords, and all cords are characterized as "external" cords, defined as a single transverse loop located just under the celomic epithelium that surrounds the gonad at this stage; and refinement of cords continues at 13.5 dpc. Although Sertoli cells acting as a organizing center in testicular cord formation has been well known (3) and studies in knockout mouse models have revealed several genes associated with testicular cord formation (7–10), how these cell types assemble into a functional organ remains to be explored (2, 11).

Proteomics technology has been widely used in postnatal testis development and function research in mice (12–16). Two proteomics studies have been carried out in the fetal gonads in mice, and identified more than 1000 proteins expressed in gonads (17, 18), however, the temporal proteome changes have not been elucidated during gonadogenesis. Additionally, mRNA abundance may not always predict the quantity of the corresponding functional protein, and pro-

[1] The abbreviations used are: dpc, days post coitum; IF, immunofluorescence; ROS, reactive oxygen species; TMT, tandem mass tag; SCX, strong cation exchange; DE, differentially expressed; STIM1 (*Stim1*), stromal interaction molecule 1; NAC, *N*-acetylcysteine.

teomic approach can provide a systemic view of protein level regulation in a large scale (18). Therefore, this study aimed to obtain a better understanding of male gonadogenesis by establishing a first temporal proteomic profile during the initiation of gonad development in male mice. After confirming the specific time point by immunofluorescence (IF) staining, we performed a comparative proteomic analysis of samples of male mouse gonads obtained at 11.5, 12.5, and 13.5 dpc. Bioinformatics analysis and functional studies demonstrate that reactive oxygen species (ROS) regulation in Sertoli cells may be important for testicular cord formation, and functional characterizing the of stromal interaction molecule 1 (stim1), a Sertoli cell specific protein, supported this hypothesis. Our categorized protein lists can serve as a useful resource for further exploring the molecular mechanisms involved in gonadal development.

EXPERIMENTAL PROCEDURES

Animals and Sample Collection—All animal experiments were approved by the Ethics Committee of Nanjing Medical University (China). Timed mating of the ICR strain with noon of the day on which the mating plug was observed designated 0.5 dpc. The sex of the gonad could be determined by observation at 12.5 and 13.5 dpc. At 11.5 dpc, the embryos were genotyped to determine the sex using primers to detect *Sry*, and *β-actin* was used as an internal control. The following primers were used: *Sry*, GTTCAGCCCTACAGCCACAT (forward) and CCACGGGACCACACCATAAA (reverse); *β-actin*, GGCTGTATTCCCCTCCATCG (forward) and TCCTATGGGAGAACGGCAGA (reverse). Approximately 800 gonad pairs at 11.5 dpc, 500 gonad pairs at 12.5 dpc, and 500 gonads pairs at 13.5 dpc (with mesonephroi removed) were resected from male mouse embryos for use in the proteomics screen.

Gonad Culture—Gonads of 12.0 dpc embryos were isolated by dissection in physiological saline at room temperature, and collected into warmed Dulbecco's Minimal Eagle's Medium (DMEM) containing 10% fetal calf serum (FCS) and 50 μg/ml ampicillin at 37 °C with 5% CO_2. *Stim1*-Translation-Blocking-Vivo-Morpholino (Oligo Sequence CAAGACGGGCGCACACATCCATGAC) and Standard Control (Oligo Sequence CCTCTTACCTCAGTTACAATTTATA) were purchased from Gene Tools, LLC. After culture for 30 h, gonads were collected for further study. ROS and ATP detection were performed by ROS advanced fluoro assay kit (Genmed Scientifics, DE) and ATP Assay Kit (Beyotime, Beijing, China).

Protein Extraction and Digestion—Gonads from 11.5, 12.5, and 13.5 dpc were kept separate and collected in ice-cold PBS, and proteins were extracted using protein extraction buffer consisting of 7 M urea, 2 M Thiourea, 65 mM dithiothreitol (DTT) and 1% (v/v) protease inhibitor mixture. After incubation for 1 h on ice (vortexing every 10 min), the supernatants were collected by centrifugation at 40,000 × *g* for 60 min at 4 °C. The protein content of the supernatants was measured using Bradford assay. Prior to tandem mass tag (TMT) labeling, 70 μg protein was used for tryptic digestion for each TMT Label reagent. The cysteine residues were reduced with 200 mM DTT for 1 h at 56 °C and alkylated in 375 mM IAA for 45 min at RT in the dark, followed by digestion overnight at 37 °C with trypsin in a 1:50 enzyme:protein ratio. The experiments were repeated for four times, with 12 samples in total for gonads of three stages.

TMT Labeling—TMT 6-plex labeling was performed according to the manufacturer's protocol with minor modifications. In brief, TMT Label Reagents were equilibrated to room temperature. Each aliquot was suspended in 41 μl of anhydrous acetonitrile, and 42 μl of the reagent was added to the digestion dissolved in 200 mM triethylammonium bicarbonate (TEAB). After reaction at room temperature for 1 h, 8 μl of 5% hydroxylamine was added to each tube, and the mixture was incubated for another 15 min. The aliquots were then combined, and the pooled sample was evaporated in a vacuum. A total of two TMT six-plex labeling experiments were performed, and each labeled six samples involving two replicates.

Strong Cation Exchange (SCX) Fractionation—The labeled peptide mixture was resuspended in SCX chromatography Buffer A (10 mM NH_4COOH and 5% ACN; pH 2.7) and loaded onto an SCX column (1 mm internal diameter × 10 cm, packed with Poros 10S; Dionex, Sunnyvale, CA) in an UltiMate® 3000 HPLC systems at a flow rate of 50 μl/min. The following linear gradient was used: 0% to 56% B (800 mM NH_4COOH and 5%ACN, pH 2.7) in 30 min; 56% to 100% B for 1 min; 100% B for 3 min; 100% to 0% B for 1 min; and 0% B for 20 min before the next run. The effluents were monitored at 214 nm based on the UV light trace, and fractions were collected every 2 min (19–21).

Mass Spectrometry Analysis—Seventeen fractions were sequentially loaded onto a μ-precolumn™ cartridge (0.3 × 5 mm^2, 5 μm, 100 Å; Dionex) at a flow rate of 20 μl/min. The trap column effluent was then transferred to a reverse-phase microcapillary column (0.075 × 150 mm^2, Acclaim® PepMap100 C18 column, 3 μm, 100 Å; Dionex). The reverse-phase separation of peptides was performed using buffer A (2% ACN and 0.5% acetic acid) and buffer B (80% ACN and 0.5% acetic acid); a 193-min gradient (4% to 9% buffer B for 3 min, 9% to 33% buffer B for 170 min, 33% to 50% buffer B for 10 min, 50% to 100% buffer B for 1 min, 100% buffer B for 8 min, and 100% to 4% buffer B for 1 min) was used.

Peptides were detected on LTQ Orbitrap Velos (Thermo Fisher Scientific, Waltham, MA) using a data-dependent acquisition mode. The MS3 method was programmed as previously described (16). For each cycle, one full MS scan of mass/charge ratio (m/z) = 350–1800 was acquired in the Orbitrap at a resolution of 60,000. After each full scan, eight of the most intense ions were selected for collision-induced dissociation (CID) fragmentation (CE 35%), and the most intense product ion from the MS2 step was selected for higher-energy collisional dissociation (HCD) fragmentation (NCE 68%). Wideband activation was enabled. Lock mass, with siloxane (m/z = 445.120025), was used in all runs to calibrate orbitrap MS precursor masses. The mass spectrometry proteomics data are available via ProteomeXchange with identifier PXD002563.

Protein Identification and Quantification—The raw files were processed with MaxQuant (22) software (version 1.2.2.5) using the International Protein Index (IPI) (23) mouse proteome database (version 3.83; 60,010 entries). A database of common contaminants embedded in MaxQuant (248 entries) was also included for quality control. The reverse strategy was used to estimate the false discovery rate. Trypsin/P was set as proteolytic enzyme and, a maximum of two missed cleavage sites was permitted. A minimum peptide length of six was required. Except for TMT labels, carbamidomethyl (C) was set as fixed modification. Variable modifications were oxidation (M) and acetyl (protein N-term). The mass tolerance for precursor ions was set to 20 ppm at the first search as applied in MaxQuant for initial mass recalibration. For the main search, the mass tolerance for precursor ions was set to 6 ppm. The mass tolerance for MS/MS fragment ions was set to 0.5 Da. Protein quantification was calculated by combining MaxQuant identification results according to Libra algorithm (24). In brief, each channel of reporter ion intensity was normalized by the sum of the signals in the corresponding channels. For each peptide, spectra with intensities that deviated from the mean by over 2 Sigma were removed. Each peptide channel was then re-normalized by the sum across channels. The protein intensity was calculated as the median of normalized intensity of the corresponding peptides. For the identification of differentially expressed (DE) proteins among

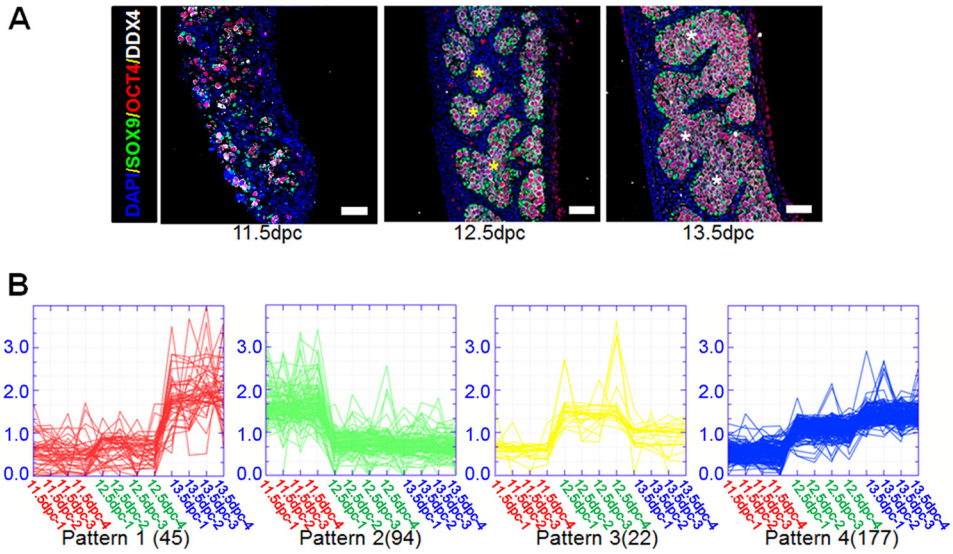

FIG. 1. **Expression patterns of differentially expressed proteins during testicular cords formation.** *A*, At 11.5 dpc, pre-Sertoli cells labeled by SOX9 and germ cells labeled by OCT4 and DDX4 were evenly distributed. From 12.5 dpc, germ cells started forming clusters (asterisks, yellow) and were surrounded by Sertoli cells. At 13.5 dpc, Sertoli cells enclosed germ cell populations in distinct testicular cords (asterisks, white). Scale bars: 50 μm. *B*, Totally 45 DE proteins were in the cluster of Pattern 1, 94 in Pattern 2, and 22 in Pattern 3, as well as 177 in Pattern 4. For each stage, there were 4 replicates.

groups, the cutoffs of fold change and Q value were set to 2 and 0.01, respectively, using the significance analysis of microarrays (SAM) algorithm performed by J-expression (25).

Western Blot Analysis—Western blotting was performed as described previously (14, 26) with a modification. Briefly, the proteins were separated by SDS-PAGE and transferred onto a polyvinylidene difluoride membrane. The membrane was blocked with 5% nonfat milk in TBST solution for 2 h at room temperature, and incubated overnight at 4 °C with primary antibodies. The membranes were washed with TBST buffer three times and incubated at room temperature for 2 h with secondary antibodies. The signals of the detected proteins were visualized on SuperSignal* West Femto Chemiluminescent Substrate Western blotting detection system (Thermo Scientific). Information about all the antibodies used for the analysis is presented in supplemental Table S1.

IF Stlaining—Paraffin-embedded gonad sections were dewaxed and dehydrated. Endogenous peroxidase activity was arrested by incubating the sections with 3% hydrogen peroxide for 15 min. Antigen retrieval was performed by boiling samples in 0.01 M sodium citrate buffer (pH 6.0) for 10 min. The sections were incubated with 5% bovine serum albumin in PBS for 2 h at room temperature. The sections were incubated with primary antibody at 4 °C overnight. After washing with PBS, secondary antibody was applied for 2 h, and the nucleus was stained with DAPI. For whole mount staining, gonads were fixed with 4% paraformaldehyde for 30 min, blocked with 5% bovine serum albumin for 2 h and incubated with primary antibodies overnight at 4 °C, as described previously (16). On the second day, the gonads were washed thrice, and incubated with secondary antibody for 2 h, mounted on slides, and examined. Cell counting was performed by previous reported method (27, 28). Briefly, images of the three most interior sections of each whole mount-stained gonad were collected using the confocal microscope (LSM 710, Carl Zeiss, Oberkochen, Germany). To avoid counting the same cells in consecutive sections, sections were spaced at least 5 mm intervals. Cells with positive signals were counted in three sections and averaged for each gonad. Sample number for each group was at least 3.

RESULTS

Identification of Specific Time Points During the Formation of Testicular Cords—IF analysis was used to identify the dynamic changes involved in early testis development (Fig. 1*A*). Germ cells were labeled with DDX4 and OCT4; and Sertoli cells, with SOX9. At 11.5 dpc, pre-Sertoli and germ cells were evenly distributed among the genital ridges. At 12.5 dpc, the Sertoli cells and germ cell clusters had begun to form individual cords. At 13.5 dpc, the testicular cords were larger, more clearly defined, and further differentiated. These findings were consistent with previous reports (5, 6). During this period, different cell linage-specific genes contributed to the functional maturation of the testicular cords to a considerable extent. The three time points involving testicular cord development were used in subsequent proteomic experiments.

Bioinformatics Analysis of DE Proteins Reveals Possible Important Roles of Sertoli Specific Genes in Male Gonadogenesis—Embryonic testis at three time points (11.5, 12.5, and 13.5 dpc) were collected with the removal of mesonephros under microscope to construct a quantitative proteome profile of testicular cord formation during early gonadal development. With TMT labeling and mass spectrometry analysis, 4070 proteins were identified in embryonic testis, of which 4049 were identified at 11.5 dpc, 4056 at 12.5 dpc, and 4051 at 13.5 dpc. Totally 4032 proteins were identified in all three time points. Of these proteins, 338 were found to be DE (supplemental Table S2) during testicular cord formation. Subcellular distributions of DE proteins were annotated using gene ontologies (GO) by database for annotation, visualization, and integrated discovery (DAVID) (29, 30). As shown in

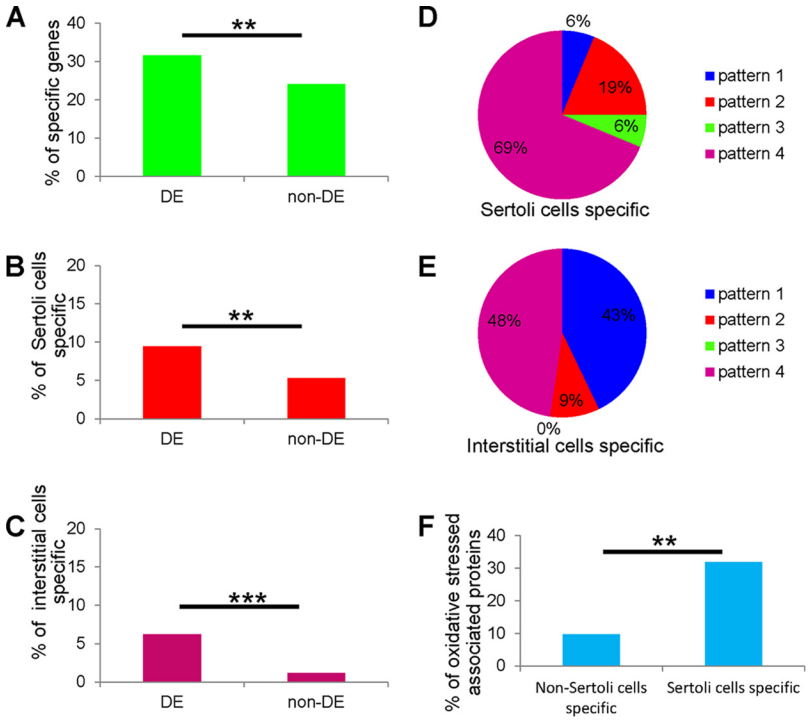

FIG. 2. **Bioinformatics analysis of the comparative proteomic profile.** *A*, The percentage of lineage specific genes in total in DE proteins was markedly higher than that in non-DE proteins ($p = 0.0022$). *B*, *C*, In the Sertoli and interstitial cell specific genes, their percentages in DE proteins were significantly higher than those in non-DE proteins. *D*, *E*, Pie chart showed that the Sertoli and interstitial cell specific genes were mainly mapped to Pattern 4. *F,* The percentage of oxidative stress-associated proteins in Sertoli cells specific proteins was significantly higher than those in the non-Sertoli cells specific proteins in Pattern 4. Statistical analysis was performed by Chi-square test and Chi-square test with Yate correction ** $p < 0.01$, *** $p < 0.001$.

supplemental Fig. S1, the largest proportion of DE proteins identified was annotated as cytoplasm (191), followed by membrane (138), nucleus (85), and mitochondrion (52).

Based on expression patterns, using k-means clustering algorithm (31, 32), these 338 DE proteins were classified into four clusters(supplemental Table S3) by J-Express software (25). The four clusters indicated four distinct expression patterns (Fig. 1*B*): increase at 13.5 dpc (45 proteins, Pattern 1), decrease at 12.5 dpc and remain unchanged at 13.5 dpc (94 proteins, Pattern 2), increase at 12.5 dpc but decrease at 13.5 dpc (22 proteins, Pattern 3), and steady increase across all time points (177 proteins, Pattern 4).

In this study specific cell lineages were not separated, because of the large amount of proteins required for proteomic studies, it is difficult to get enough proteins of specific cell lineage in embryonic gonad for proteomics analysis. However, Jameson *et al.* analyzed transcriptome of each cell lineage in embryonic testis, and according to mRNA expression values, they assembled the lineage specific genes that were specifically enriched in each cell lineage, including Sertoli, interstitial cells, germ cells, and endothelial cells, relative to the other lineages in embryonic testis (33). Although mRNA expression does not necessarily translate to protein levels, studies have shown that as high as 65–79% (correlation of r^2, 0.65–0.79) of the protein level changes can be explained by mRNA levels (34, 35). The lineage-specific gene expression at mRNA levels implies potential important functions of certain gene in the corresponding lineage. Analysis of the distribution of these lineage specific genes showed that the lineage specific genes tended to be differentially-expressed across developmental stages at protein level, there was significant enrichment of lineage specific genes as a total in DE proteins compared with non-DE proteins (31.66% versus 24.14%, $p < 0.01$, Fig. 2*A*). Furthermore, we analyzed the distribution of lineage specific genes from each lineage separately (supplemental Table S4) and found that for the Sertoli and interstitial cell specific genes, there was significant enrichment in the DE proteins compared with those in non-DE proteins (9.47% *versus* 5.33%, $p < 0.01$ and 6.21% *versus* 1.18%, $p < 0.001$, respectively, Fig. 2*B*, 2*C*). And no significant enrichment was observed for endothelial cell and germ cell specific genes ($p > 0.05$, supplemental Fig. S2). In addition, among the DE proteins, Sertoli cell specific genes (69%) and interstitial cells specific genes (48%) mainly have steady increased expression during testicular cord formation at protein level (Pattern 4; Fig. 2*D*, 2*E*), which indicated the importance of these proteins in testicular cord formation. To verify results of the TMT quantification, several proteins with commercially available antibodies from the cluster of Pattern 4 were chosen for Western blot analysis. As shown in supplemental Fig. S3, Western blot and TMT quantification showed consistent results. Thus, this quantitative proteomic results are of high confidence.

As Sertoli cell and interstitial cell specific genes are enriched in DE proteins during testis development. We annotated the functions of these proteins according to different expression patterns by the Pathway Studio software, and found that in Pattern 4, there was significant enrichment of oxidative stress-associated proteins in proteins with Sertoli cell specific gene expression compared with those in the rest

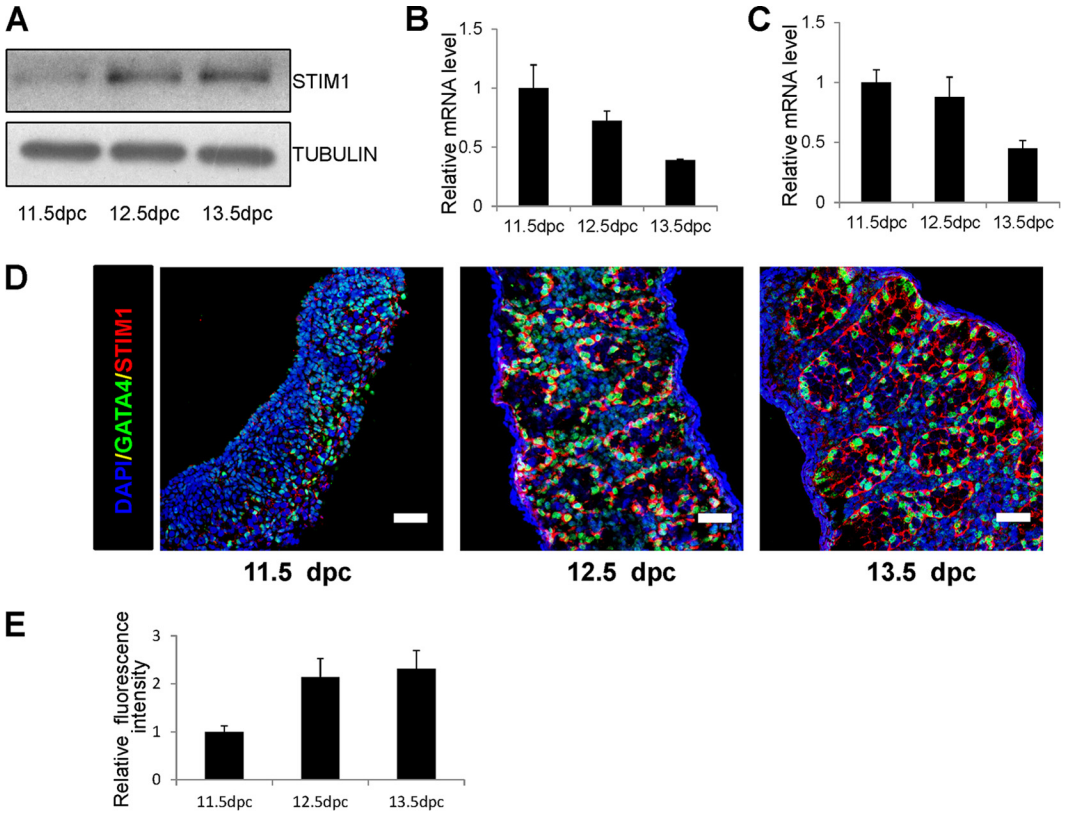

FIG. 3. **Expression of *Stim1* during gonadogenesis.** *A*, Western blot data showed weak expression of STIM1 at 11.5 dpc male gonads, but increase at 12.5 and 13.5 dpc. *B*, *C*, Relative mRNA level of *Stim1* from our study and Jameson's microarray, respectively. *D*, Representative images of co-immunostaining of GATA4 and STIM1 at 11.5, 12.5 and 13.5 dpc male gonads. Scale bars: 50 μm. *E*, Quantification of STIM1 at 11.5, 12.5, and 13.5 dpc male gonads by fluorescence intensity.

of Pattern 4 proteins (31.82% *versus* 9.68%, $p < 0.01$) (Fig. 2*F,* supplemental Table S5). In the interstitial cell lineage, however, there was no such enrichment. These data suggest that regulation of oxidative stress in Sertoli cells might be important in the regulation of testicular cord formation during male gonadal development.

Expression and Distribution of Stim1 in Male Gonads—As bioinformatics analysis showed possible roles of oxidative stress regulation in testicular cord formation, we selected STIM1, an oxidative stress-associated protein from cluster of Pattern 4 of steady increased expression with enrichment of Sertoli cell specific proteins, for further functional study. Western blot data indicated that, at protein level, STIM1 was weakly expressed at 11.5 dpc, but increased at 12.5 and 13.5 dpc (Fig. 3*A*), which was consistent with our TMT quantification. However, in contrast to its protein level, we found that *Stim1* decreased at 13.5 dpc at mRNA level according to real-time reverse transcriptase polymerase chain reaction (real-time PCR) analysis (Fig. 3*B*). In addition, our real-time PCR results were highly consistent with Jameson's microarray data (Fig. 3*C*). Together, these results showed post-transcriptional regulations during testicular cord development, and that mRNA and protein of the same gene may exhibit discrepant or even reversed temporal expression patterns, with *Stim1* as a good example of this phenomenon. Thus, it is crucial to study the functions of genes at protein level, and mRNA level studies only are not enough to elucidate mechanisms of male gonadogensis.

Next, we performed IF staining to analyze the STIM1 distribution in embryonic testis. As shown in Fig. 3*D*, STIM1 is a Sertoli cell specific protein, and is mainly expressed in the cytoplasm of Sertoli cells. Quantification of the fluorescence intensity of STIM1 (Fig. 3*E*) showed similar trend of expression changes during embryonic testis development as those shown in the Western blot (Fig. 3*A*) and the TMT quantification.

Suppression of Stim1 causes severe phenotypes in gonadogenesis—To explore the function of *Stim1* in gonadogenesis, we used morpholino oligo against *Stim1*, and successfully suppressed *Stim1* translation *in vitro*. Western blotting analysis revealed about 55% suppression efficiency (Fig. 4*A*, 4*B*).

After *Stim1* knockdown, severe disruption in testicular cord development was observed. As shown in Fig. 5, the testicular cords in the knockdown group were disorganized and showed significant reduction in the number of Sertoli cells (labeled by SOX9 and WT1; Fig. 5*A*, 5*B*, 5*G*, 5*H*), and germ cells (labeled by OCT4 and DDX4; Fig. 5*A*–5*C*, 5*E*, 5*I*, 5*J*).

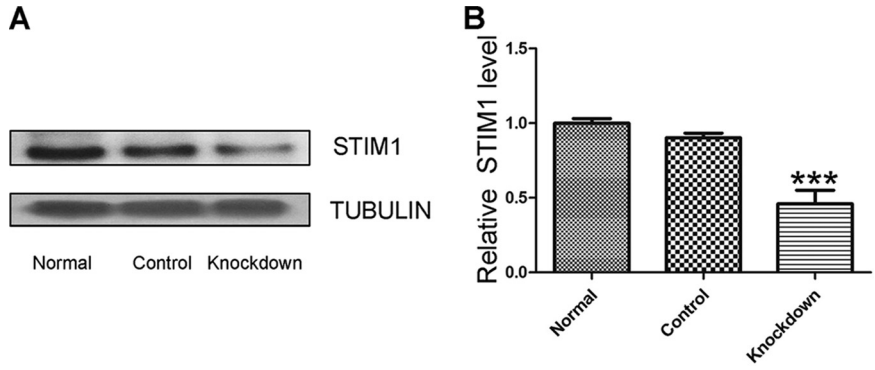

FIG. 4. ***A*, Verification of 5 μM translation-blocking vivo-morpholino interference efficiency on the STIM1 protein level.** *B*, Western blot results showed about 55% suppression efficiency. Statistical analysis was performed by one way ANOVA. *** $p < 0.001$.

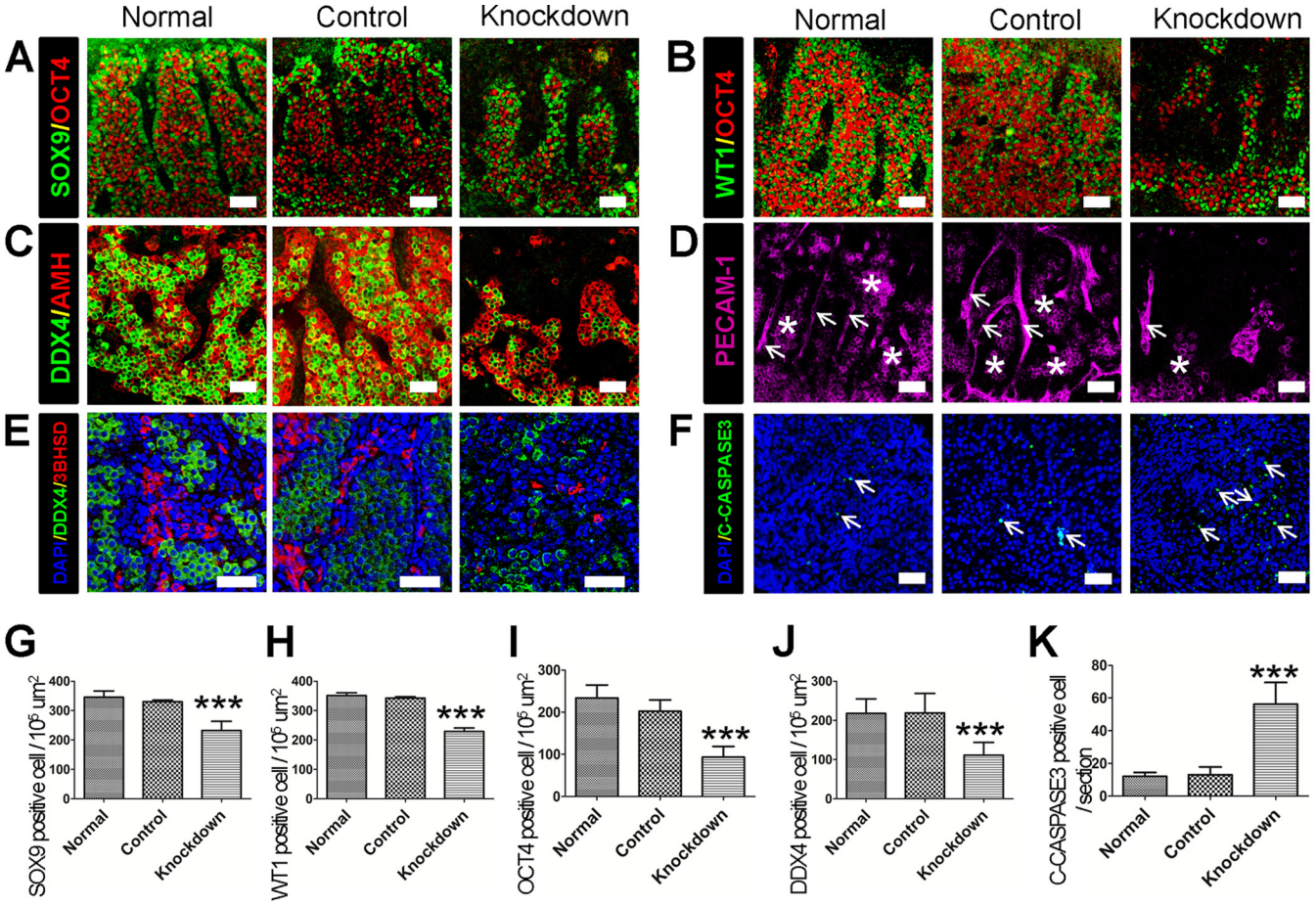

FIG. 5. **Suppression of *Stim1* leaded to defects in testicular cord formation.** In the *Stim1* knockdown group, there was an obvious reduction in the Sertoli cells labeled by SOX9 (*A*) and WT1 (*B*) and germ cells labeled by OCT4 (*A*, *B*) and DDX4 (*C*, *E*). Statistical data were displayed in (*G–J*). *Stim1*-deficient gonads showed failed angiogenesis (*D*) and development of interstitial cells labeled by 3β-HSD (*E*). PECAM1 was distributed in both germ cells (*D*, asterisks) and endothelial cells (*D*, arrows). Cell apoptosis test results showed that the cleaved CASPASE3-positive cells were significantly higher in the *Stim1* knockdown group (*F*, arrows), compared with the normal and control groups. Statistical data were presented in (K). Statistical analysis was performed by one way ANOVA. n≥ 3. Scale bars: 50 μm.*** $p < 0.001$.

Moreover, to test whether knockdown of *Stim1* in Sertoli cells could affect the development of endothelial cells and interstitial, we also examined the histological architecture of PECAM1-labeled endothelial cells (Fig. 5*D*) and 3β-HSD-labeled interstitial cells (Fig. 5*E*). Both cell types were malformed and decreased in numbers after *Stim1* knockdown in Sertoli cells. To determine the reason for this reduction in cell number, we detected cell proliferation and apoptosis by detecting the expression levels of cleaved KI67 and CASPASE-3, respectively. There was a significantly higher number of cleaved CASPASE-3-positive cells in the knockdown group (Fig. 5*F*, 5*K*) than in the normal and control

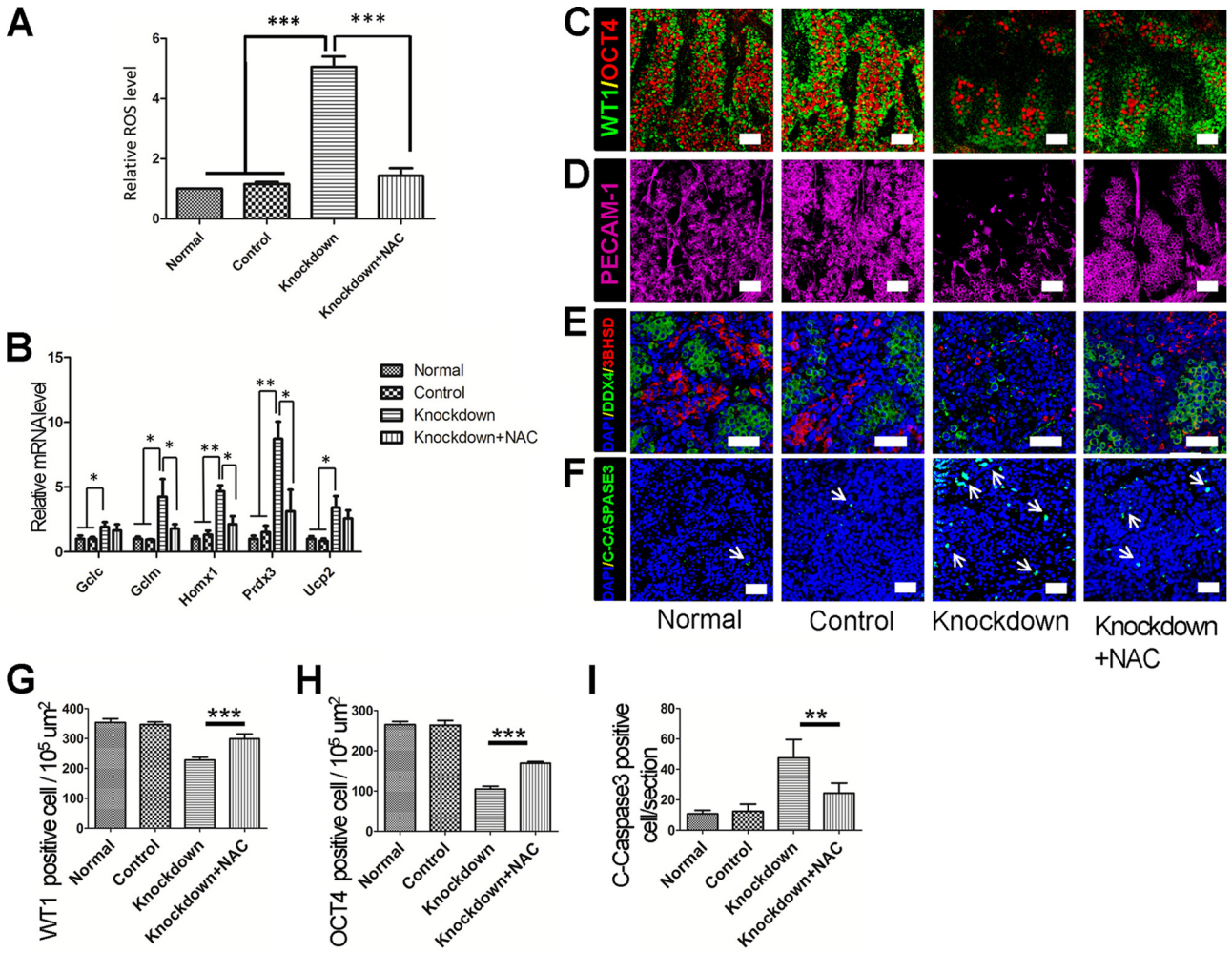

FIG. 6. **Antioxidant treatment can partially rescue testicular cord disruption in *Stim1*-deficient gonads.** There was a significant increase in the ROS level in the knockdown group, which was reduced by NAC treatment (*A*). The antioxidant response genes *Gclc*, *Gclm*, *Homx1*, *Prdx3,* and *Ucp2* were elevated in the knockdown group and *Gclm*, *Homx1,* and *Prdx3* were markedly downregulated by NAC treatment (*B*). The numbers of Sertoli (*C*, *G*) and germ cells (*C*, *H*) were significantly increased in the NAC treatment knockdown group compared with the knockdown group. The loss of endothelial (D) and interstitial (*E*) cells in the knockdown group was reversed after treatment with NAC. Cell apoptosis marked by cleaved CASPASE-3 (F, I, arrows) showed obvious reduction following treatment with NAC. Statistical analysis was performed by one way ANOVA. n ≥ 3. Scale bars: 50 μm. * $p < 0.05$, ** $p < 0.01$, *** $p < 0.001$.

groups, whereas there was no obvious change in the number of KI67-positive cells between the knockdown, normal, and control groups (supplemental Fig. S4*A*, S4*B*), suggesting that the reduction in the cell number was a result of cell apoptosis.

Suppression of Stim1 Showed no Obvious Change in Phenotype in Early Female Gonads—Due to the phenotypes caused by *Stim1* knockdown in male gonads, we wondered whether *Stim1* played a role in female gonads. Interestingly, we found no obvious morphological changes in the female knockdown group compared with the normal and control female gonads (supplemental Fig. S5*A*, S5*B*). Western blot analysis showed different expression patterns of STIM1 between XY and XX gonads, with an up-regulated expression pattern in XY (Fig. 3*A*) and a down-regulated expression at 13.5 dpc in XX (supplemental Fig. S6). These results indicate that *Stim1* might not be required for female gonads differentiation at this stage.

Reduction of Increased Oxidative Stress Can Partially Rescue Phenotypes Caused by Stim1 Knockdown—As *Stim1* is related to oxidative stress, we sought to assess whether oxidative stress could contribute to the phenotypic defects. The ROS content was markedly higher in the knockdown group than that in the normal and control groups ($p < 0.001$) (Fig. 6*A*). Furthermore, the antioxidant response genes *Gclc*, *Gclm*, *Homx1*, *Prdx3*, and *Ucp2* were significantly up-regulated in the knockdown group (Fig. 6*B*), suggesting that *Stim1* deficiency causes constitutive oxidative stress. However, when the knockdown group was treated with the antioxidant scavenger *N*-acetylcysteine (NAC), the ROS levels markedly decreased in the knockdown group, although they did not

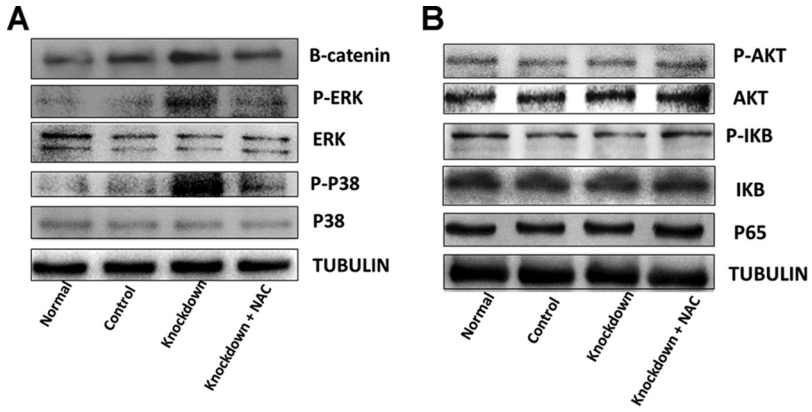

FIG. 7. **Western blot analysis of signaling pathways involved in ROS.** Western blot data indicated that β-catenin, ERK, and P38 were activated, and NAC treatment reduced their expression levels (*A*). Akt and NF-kB pathways showed no apparent alterations in the knockdown and NAC treated knockdown groups (*B*).

reach the normal levels (Fig. 6*A*). And addition of NAC led to a reduction in the expression levels of the antioxidant response genes, although the reduction in the *Gclc* and *Ucp2* levels was not significant (Fig. 6*B*). The defects in the testicular morphology were partially rescued after treatment with NAC (Fig. 6*C*–6*I*). The numbers of Sertoli and germ cells in the NAC-treated knockdown group were significantly higher than those in the knockdown group (Fig. 6*C*, 6*G*, 6*H*). The numbers of endothelial (Fig. 6*D*) and interstitial (Fig. 6*E*) cells were higher in the NAC-treated knockdown group than in the knockdown group. Additionally, we observed that the number of cleaved CASPASE-3-positive cells was lower in the NAC-treated knockdown group than in the knockdown group (Fig. 6*F*, 6*I*). Together, these results demonstrate that the aberrant elevation of ROS can cause defects in testis development, whereas the reduction of ROS can partially rescue them.

ROS is well known to activate many important signaling pathways including mitogen-activated protein kinase (MAPK) cascades, nuclear factor-kB (NF-kB), P-I-3-kinase-Akt, and wnt/β-catenin (36–38). We found that β-catenin, ERK, and P38 were activated (Fig. 7*A*), whereas NAC addition reduced their expression levels. The Akt and NF-kB pathways showed no obvious changes in both knockdown and NAC treatment knockdown groups (Fig. 7*B*).

DISCUSSION

Emerging evidence has illustrated that Sertoli, interstitial, and endothelial cells all participate in the development of testicular cords. Deletions of genes that are specifically expressed in the Sertoli and interstitial cells have been shown to cause severe disruption of testicular cords, and blocking the migration of endothelial cells can impede organization of the testis (10, 39, 40). Testicular cords appear normal in mutant mice lacking germ cells, indicating that germ cells are not vital for cord formation (41). In order to get a systemic view of regulation of testicular cord formation at protein levels, we generated a comparative proteomic profile of male mouse gonads at three time points spanning the critical period for testicular cord formation. Several of the DE proteins obtained in our profile have been previously reported to function in gonadal development (supplemental Table S6). For example, *Amh* (anti-Müllerian hormone) is crucial for regression of the Müllerian duct and for the promotion of testis differentiation (42, 43).

Comparison with lineage specific genes compiled by Jameson *et al.* (33) based on mRNA expression data showed that Sertoli cell specific genes were enriched in Pattern 4 with steady increased expression. Oxidative stress related proteins were over-represented in Sertoli cell specific DE proteins; therefore, these results suggest that oxidative stress regulation in Sertoli cells may be important to the formation of testicular cords. In order to verify this hypothesis, STIM1, a Sertoli cell specific protein in Pattern 4 related to oxidative stress regulation, was selected for further study. STIM1 is a transmembrane ER protein containing multiple functional domains, and it serves as an ER Ca^{2+} sensor and activator of store-operated Ca^{2+} entry (SOCE) (44–46). Studies have shown that *Stim1* is associated with oxidative stress and mitochondrial bioenergetics (47). We found that suppression of *Stim1* in Sertoli cells in the cultured testis *in vitro* increased ROS production and caused a global disruption of gonads, evidenced by disorganized testicular cord formation, obstruction of angiogenesis, and loss of interstitium. The severe phenotypes observed by *Stim1* knockdown demonstrated that *Stim1* in Sertoli cells played a essential role in testicular cord formation. Further study indicated that molecules downstream of ROS generation, such as β-catenin, ERK, and P38, were significantly activated in the knockdown group, and treatment of the knockdown group with the antioxidant scavenger NAC could inhibit ROS production, consequently down-regulating the expression of β-catenin, ERK, and P38, and partially rescuing the defects in testicular cord formation.

ROS is an essential regulator of cell processes and is generated in all cells. Although ROS is well known to be toxic, they also function as signaling molecules (48). Oxidative stress during spermatogenesis is generally associated with male infertility. Mice deficient in the transcription factor nuclear factor-erythroid 2-related factor 2 (*Nrf2*), which regulates the basal and inducible transcription of genes encoding enzymes important for protection against ROS, have been

shown to have disruptive spermatogenesis in an age-dependent manner (49), whereas moderate ROS levels are beneficial for the self-renewal of mouse spermatogonial stem cell (SSC) (50). In humans, physiological ROS is beneficial for the cyclic waves of spermatogenesis, whereas excess ROS are harmful and can cause human infertility (51–53). Our present study indicated that aberrant elevation of ROS caused by suppression of STIM1 in Sertoli cells in early mouse gonads could impair testicular cord formation.

Wnt/β-catenin signaling is one of the fundamental mechanisms that direct cell proliferation, cell polarity, and cell fate specification during embryonic development and tissue homeostasis (54, 55). Activation of the Wnt pathway leads to translocation of β-catenin into the nucleus and formation of a heterodimeric complex of β-catenin with the Tcf/Lef family of DNA-binding proteins; this complex then regulates the transcription of downstream target genes such as *Myc* and *Cyclin D1* (56, 57). In the last few years, the role of β-catenin in fetal testis development has been gradually established (58). It has been shown that the constitutively active form of β-catenin in embryonic Sertoli cells in mouse causes testis malformation, including testicular cord disruption and germ cell depletion (59, 60). It should be noted that our *ex vivo* gonad culture experiments are not substitutes of *in vivo* experiments, the use Stim1 knockout mouse models are preferred in future studies in order to elucidate its functions in testis development. With the *ex vivo* studies, our results demonstrated that *Stim1* could regulate β-catenin in gonadal development by ROS signaling.

In conclusion, our comparative proteomic profile of mouse testicular cord formation and functional studies revealed the important roles of oxidative stress regulation in Sertoli cells in the testicular cord formation during early testis development.

Acknowledgments—We thank Peter Koopman from Institute for Molecular Bioscience, the University of Queensland and Blanche Capel from Department of Cell Biology, Duke University Medical Center for technical assistance.

* This work was supported by grants from the Chinese National Natural Science Foundation (81222006) and the 973 program (2015CB943003 and 2011CB944304).

Ⓢ This article contains supplemental Tables S1 to S6 and Figs. S1 to S6.

§ To whom correspondence should be addressed: Department of Histology and Embryology, Nanjing Medical University, State Key Laboratory of Reproductive Medicine, Nanjing Medical University, Nanjing 210029 China. Dr. Xuejiang Guo, Tel.: 86-25-86862038; Fax: 86-25-86862908; E-mail: guo_xuejiang@njmu.edu.cn; Dr. Zuomin Zhou, Tel.: +86-25-86862908, Fax: +86-25-86862908, E-mail: zhouzm@njmu.edu.cn.

¶ These authors contributed equally to the work.

REFERENCES

1. Brennan, J., and Capel, B. (2004) One tissue, two fates: molecular genetic events that underlie testis versus ovary development. *Nat. Rev. Genet.* **5,** 509–521
2. Cool, J., DeFalco, T., and Capel, B. (2012) Testis formation in the fetal mouse: dynamic and complex de novo tubulogenesis. *Wiley Interdiscip. Rev. Dev. Biol.* **1,** 847–859
3. Svingen, T., and Koopman, P. (2013) Building the mammalian testis: origins, differentiation, and assembly of the component cell populations. *Genes Dev.* **27,** 2409–2426
4. Wilhelm, D., and Koopman, P. (2006) The makings of maleness: towards an integrated view of male sexual development. *Nat. Rev. Genet.* **7,** 620–631
5. Coveney, D., Cool, J., Oliver, T., and Capel, B. (2008) Four-dimensional analysis of vascularization during primary development of an organ, the gonad. *Proc. Natl. Acad. Sci. U.S.A.* **105,** 7212–7217
6. Cool, J., DeFalco, T. J., and Capel, B. (2011) Vascular-mesenchymal cross-talk through Vegf and Pdgf drives organ patterning. *Proc. Natl. Acad. Sci. U.S.A.* **108,** 167–172
7. Brennan, J., Tilmann, C., and Capel, B. (2003) Pdgfr-alpha mediates testis cord organization and fetal Leydig cell development in the XY gonad. *Genes Dev.* **17,** 800–810
8. Meeks, J. J., Crawford, S. E., Russell, T. A., Morohashi, K., Weiss, J., and Jameson, J. L. (2003) Dax1 regulates testis cord organization during gonadal differentiation. *Development* **130,** 1029–1036
9. Gao, F., Maiti, S., Alam, N., Zhang, Z., Deng, J. M., Behringer, R. R., Lécureuil, C., Guillou, F., and Huff, V. (2006) The Wilms tumor gene, Wt1, is required for Sox9 expression and maintenance of tubular architecture in the developing testis. *Proc. Natl. Acad. Sci. U.S.A.* **103,** 11987–11992
10. Tang, H., Brennan, J., Karl, J., Hamada, Y., Raetzman, L., and Capel, B. (2008) Notch signaling maintains Leydig progenitor cells in the mouse testis. *Development* **135,** 3745–3753
11. Ewen, K. A., and Koopman, P. (2010) Mouse germ cell development: from specification to sex determination. *Mol. Cell. Endocrinol.* **323,** 76–93
12. Zhu, Y. F., Cui, Y. G., Guo, X. J., Wang, L., Bi, Y., Hu, Y. Q., Zhao, X., Liu, Q., Huo, R., Lin, M., Zhou, Z. M., and Sha, J. H. (2006) Proteomic analysis of effect of hyperthermia on spermatogenesis in adult male mice. *J. Proteome Res.* **5,** 2217–2225
13. Paz, M., Morin, M., and Del Mazo, J. (2006) Proteome profile changes during mouse testis development. *Comp. Biochem. Physiol.* **1,** 404–415
14. Huang, X. Y., Guo, X. J., Shen, J., Wang, Y. F., Chen, L., Xie, J., Wang, N. L., Wang, F. Q., Zhao, C., Huo, R., Lin, M., Wang, X., Zhou, Z. M., and Sha, J. H. (2008) Construction of a proteome profile and functional analysis of the proteins involved in the initiation of mouse spermatogenesis. *J. Proteome Res.* **7,** 3435–3446
15. Tan, Q., Dong, D., Ye, L., and Li, R. (2009) Combined usage of cascade affinity fractionation and LC-MS/MS for the proteomics of adult mouse testis. *J. Sep. Sci.* **32,** 3871–3879
16. Zheng, B., Zhou, Q., Guo, Y., Shao, B., Zhou, T., Wang, L., Zhou, Z., Sha, J., Guo, X., and Huang, X. (2014) Establishment of a proteomic profile associated with gonocyte and spermatogonial stem cell maturation and differentiation in neonatal mice. *Proteomics* **14,** 274–285
17. Wilhelm, D., Huang, E., Svingen, T., Stanfield, S., Dinnis, D., and Koopman, P. (2006) Comparative proteomic analysis to study molecular events during gonad development in mice. *Genesis* **44,** 168–176
18. Ewen, K., Baker, M., Wilhelm, D., Aitken, R. J., and Koopman, P. (2009) Global survey of protein expression during gonadal sex determination in mice. *Mol. Cell. Proteomics* **8,** 2624–2641
19. Guo, X., Zhang, P., Qi, Y., Chen, W., Chen, X., Zhou, Z., and Sha, J. (2011) Proteomic analysis of male 4C germ cell proteins involved in mouse meiosis. *Proteomics* **11,** 298–308
20. Dayon, L., Hainard, A., Licker, V., Turck, N., Kuhn, K., Hochstrasser, D. F., Burkhard, P. R., and Sanchez, J. C. (2008) Relative quantification of proteins in human cerebrospinal fluids by MS/MS using 6-plex isobaric tags. *Anal. Chem.* **80,** 2921–2931
21. Lee, M. V., Topper, S. E., Hubler, S. L., Hose, J., Wenger, C. D., Coon, J. J., and Gasch, A. P. (2011) A dynamic model of proteome changes reveals new roles for transcript alteration in yeast. *Mol. Syst. Biol.* **7,** 514
22. Cox, J., and Mann, M. (2008) MaxQuant enables high peptide identification rates, individualized p.p.b.-range mass accuracies and proteome-wide protein quantification. *Nat. Biotechnol.* **26,** 1367–1372
23. Kersey, P. J., Duarte, J., Williams, A., Karavidopoulou, Y., Birney, E., and Apweiler, R. (2004) The International Protein Index: an integrated database for proteomics experiments. *Proteomics* **4,** 1985–1988
24. Deutsch, E. W., Mendoza, L., Shteynberg, D., Farrah, T., Lam, H., Tasman, N., Sun, Z., Nilsson, E., Pratt, B., Prazen, B., Eng, J. K., Martin, D. B.,

Nesvizhskii, A. I., and Aebersold, R. (2010) A guided tour of the Trans-Proteomic Pipeline. *Proteomics* **10,** 1150–1159
25. Dysvik, B., and Jonassen, I. (2001) J-Express: exploring gene expression data using Java. *Bioinformatics* **17,** 369–370
26. Guo, X., Shen, J., Xia, Z., Zhang, R., Zhang, P., Zhao, C., Xing, J., Chen, L., Chen, W., Lin, M., Huo, R., Su, B., Zhou, Z., and Sha, J. (2010) Proteomic analysis of proteins involved in spermiogenesis in mouse. *J. Proteome Res.* **9,** 1246–1256
27. Schmahl, J., Eicher, E. M., Washburn, L. L., and Capel, B. (2000) Sry induces cell proliferation in the mouse gonad. *Development* **127,** 65–73
28. Combes, A. N., Wilhelm, D., Davidson, T., Dejana, E., Harley, V., Sinclair, A., and Koopman, P. (2009) Endothelial cell migration directs testis cord formation. *Dev. Biol.* **326,** 112–120
29. Dennis, G., Jr., Sherman, B. T., Hosack, D. A., Yang, J., Gao, W., Lane, H. C., and Lempicki, R. A. (2003) DAVID: Database for Annotation, Visualization, and Integrated Discovery. *Genome Biol.* **4,** P3
30. Huang da, W., Sherman, B. T., and Lempicki, R. A. (2009) Systematic and integrative analysis of large gene lists using DAVID bioinformatics resources. *Nat. Protoc.* **4,** 44–57
31. Akopov, A. S., Moskovtsev, A. A., Dolenko, S. A., and Savina, G. D. (2013) [Cluster analysis in biomedical researches]. *Patol Fiziol Eksp Ter*, 84–96
32. Do, J. H., and Choi, D. K. (2008) Clustering approaches to identifying gene expression patterns from DNA microarray data. *Mol. Cells* **25,** 279–288
33. Jameson, S. A., Natarajan, A., Cool, J., DeFalco, T., Maatouk, D. M., Mork, L., Munger, S. C., and Capel, B. (2012) Temporal transcriptional profiling of somatic and germ cells reveals biased lineage priming of sexual fate in the fetal mouse gonad. *PLoS Genet.* **8,** e1002575
34. Lan, P., Li, W., Lin, W. D., Santi, S., and Schmidt, W. (2013) Mapping gene activity of Arabidopsis root hairs. *Genome Biol.* **14,** R67
35. Greenbaum, D., Colangelo, C., Williams, K., and Gerstein, M. (2003) Comparing protein abundance and mRNA expression levels on a genomic scale. *Genome Biol.* **4,** 117
36. Corbi, G., Conti, V., Russomanno, G., Longobardi, G., Furgi, G., Filippelli, A., and Ferrara, N. (2013) Adrenergic signaling and oxidative stress: a role for sirtuins? *Front. Physiol.* **4,** 324
37. Korbecki, J., Baranowska-Bosiacka, I., Gutowska, I., and Chlubek, D. (2013) The effect of reactive oxygen species on the synthesis of prostanoids from arachidonic acid. *J. Physiol. Pharmacol.* **64,** 409–421
38. Vurusaner, B., Poli, G., and Basaga, H. (2012) Tumor suppressor genes and ROS: complex networks of interactions. *Free Radic. Biol. Med.* **52,** 7–18
39. Pierucci-Alves, F., Clark, A. M., and Russell, L. D. (2001) A developmental study of the Desert hedgehog-null mouse testis. *Biol. Reprod.* **65,** 1392–1402
40. Rebourcet, D., O'Shaughnessy, P. J., Pitetti, J. L., Monteiro, A., O'Hara, L., Milne, L., Tsai, Y. T., Cruickshanks, L., Riethmacher, D., Guillou, F., Mitchell, R. T., van't Hof, R., Freeman, T. C., Nef, S., and Smith, L. B. (2014) Sertoli cells control peritubular myoid cell fate and support adult Leydig cell development in the prepubertal testis. *Development* **141,** 2139–2149
41. Buehr, M., McLaren, A., Bartley, A., and Darling, S. (1993) Proliferation and migration of primordial germ cells in We/We mouse embryos. *Dev. Dyn.* **198,** 182–189
42. Rey, R. A., and Grinspon, R. P. (2011) Normal male sexual differentiation and aetiology of disorders of sex development. *Best Pract. Res. Clin. Endocrinol. Metab.* **25,** 221–238
43. Lee, M. M., and Donahoe, P. K. (1993) Mullerian inhibiting substance: a gonadal hormone with multiple functions. *Endocr. Rev.* **14,** 152–164
44. Spassova, M. A., Soboloff, J., He, L. P., Xu, W., Dziadek, M. A., and Gill, D. L. (2006) STIM1 has a plasma membrane role in the activation of store-operated Ca(2+) channels. *Proc. Natl. Acad. Sci. U.S.A.* **103,** 4040–4045
45. Roos, J., DiGregorio, P. J., Yeromin, A. V., Ohlsen, K., Lioudyno, M., Zhang, S., Safrina, O., Kozak, J. A., Wagner, S. L., Cahalan, M. D., Velicelebi, G., and Stauderman, K. A. (2005) STIM1, an essential and conserved component of store-operated Ca2+ channel function. *J. Cell Biol.* **169,** 435–445
46. Liou, J., Kim, M. L., Heo, W. D., Jones, J. T., Myers, J. W., Ferrell, J. E., Jr., and Meyer, T. (2005) STIM is a Ca2+ sensor essential for Ca2+-store-depletion-triggered Ca2+ influx. *Curr. Biol.* **15,** 1235–1241
47. Henke, N., Albrecht, P., Pfeiffer, A., Toutzaris, D., Zanger, K., and Methner, A. (2012) Stromal interaction molecule 1 (STIM1) is involved in the regulation of mitochondrial shape and bioenergetics and plays a role in oxidative stress. *J. Biol. Chem.* **287,** 42042–42052
48. D'Autréaux, B., and Toledano, M. B. (2007) ROS as signalling molecules: mechanisms that generate specificity in ROS homeostasis. *Nat. Rev. Mol. Cell Biol.* **8,** 813–824
49. Nakamura, B. N., Lawson, G., Chan, J. Y., Banuelos, J., Cortés, M. M., Hoang, Y. D., Ortiz, L., Rau, B. A., and Luderer, U. (2010) Knockout of the transcription factor NRF2 disrupts spermatogenesis in an age-dependent manner. *Free Radic. Biol. Med.* **49,** 1368–1379
50. Morimoto, H., Iwata, K., Ogonuki, N., Inoue, K., Atsuo, O., Kanatsu-Shinohara, M., Morimoto, T., Yabe-Nishimura, C., and Shinohara, T. (2013) ROS are required for mouse spermatogonial stem cell self-renewal. *Cell Stem Cell* **12,** 774–786
51. Ebisch, I. M., Thomas, C. M., Peters, W. H., Braat, D. D., and Steegers-Theunissen, R. P. (2007) The importance of folate, zinc and antioxidants in the pathogenesis and prevention of subfertility. *Hum. Reprod. Update* **13,** 163–174
52. Lavranos, G., Balla, M., Tzortzopoulou, A., Syriou, V., and Angelopoulou, R. (2012) Investigating ROS sources in male infertility: a common end for numerous pathways. *Reprod. Toxicol.* **34,** 298–307
53. Guerriero, G., Trocchia, S., Abdel-Gawad, F. K., and Ciarcia, G. (2014) Roles of reactive oxygen species in the spermatogenesis regulation. *Front Endocrinol.* **5,** 56
54. Logan, C. Y., and Nusse, R. (2004) The Wnt signaling pathway in development and disease. *Annu. Rev. Cell Dev. Biol.* **20,** 781–810
55. Clevers, H. (2006) Wnt/beta-catenin signaling in development and disease. *Cell* **127,** 469–480
56. Tetsu, O., and McCormick, F. (1999) Beta-catenin regulates expression of cyclin D1 in colon carcinoma cells. *Nature* **398,** 422–426
57. He, T. C., Sparks, A. B., Rago, C., Hermeking, H., Zawel, L., da Costa, L. T., Morin, P. J., Vogelstein, B., and Kinzler, K. W. (1998) Identification of c-MYC as a target of the APC pathway. *Science* **281,** 1509–1512
58. Lombardi, A. P., Royer, C., Pisolato, R., Cavalcanti, F. N., Lucas, T. F., Lazari, M. F., and Porto, C. S. (2013) Physiopathological aspects of the Wnt/beta-catenin signaling pathway in the male reproductive system. *Spermatogenesis* **3,** e23181
59. Chang, H., Gao, F., Guillou, F., Taketo, M. M., Huff, V., and Behringer, R. R. (2008) Wt1 negatively regulates beta-catenin signaling during testis development. *Development* **135,** 1875–1885
60. Maatouk, D. M., DiNapoli, L., Alvers, A., Parker, K. L., Taketo, M. M., and Capel, B. (2008) Stabilization of beta-catenin in XY gonads causes male-to-female sex-reversal. *Hum. Mol. Genet.* **17,** 2949–2955